Analytica Chimica Acta 1242 (2023) 340716

Contents lists available at ScienceDirect

Analytica Chimica Acta

journal homepage: www.elsevier.com/locate/aca

Sandwich-like electrochemical aptasensing of heat shock protein 70 kDa (HSP70): Application in diagnosis/prognosis of coronavirus disease 2019 (COVID-19)

Masoud Negahdary [a,*], Mario Hiroyuki Hirata [b], Solange Kazumi Sakata [c], Rozana Mesquita Ciconelli [d], Gisele Medeiros Bastos [d], Jéssica Bassani Borges [d], Helena Strelow Thurow [d], Alceu Totti Silveira Junior [a], Marcelo Ferraz Sampaio [d], Larissa Berretta Guimarães [d], Bruno Sussumu Maeda [d], Lúcio Angnes [a,**]

[a] Department of Fundamental Chemistry, Institute of Chemistry, University of São Paulo, Av. Prof. Lineu Prestes, 748, 05508-000, São Paulo, Brazil
[b] Department of Clinical and Toxicological Analyses, School of Pharmaceutical Sciences, University of Sao Paulo, Av Prof Lineu Prestes 580, 05508-000, São Paulo, Brazil
[c] Nuclear and Energy Research Institute, National Commission of Nuclear Energy (IPEN/CNEN - SP), São Paulo, SP, 05508-000, Brazil
[d] Research and Education Division, Hospital A Beneficência Portuguesa de São Paulo, São Paulo, Brazil

HIGHLIGHTS

- First biosensing application of HSP70 for diagnosis/prognosis of COVID-19 developed.
- Sandwich-like design equipped with reduced graphene oxide (rGO), Acropora-like gold (ALG) nanostructure, and aptamer-AuNPs.
- Aptasensor confirmed a wide linear detection range (5 pg mL^{-1} - 75 ng mL^{-1}) and a desirable LOD (2 pg mL^{-1}).
- Forty real plasma samples of hospitalized COVID-19 patients were analyzed and compared to the RT-PCR method.

ARTICLE INFO

Keywords:
Coronavirus disease 2019 (COVID-19)
Heat shock protein 70 kDa (HSP70)
Aptasensor
Bioelectrochemistry
Reduced graphene oxide (rGO)
Gold nanomaterials

ABSTRACT

In this research, by using aptamer-conjugated gold nanoparticles (aptamer-AuNPs) and a modified glassy carbon electrode (GCE) with reduced graphene oxide (rGO) and Acropora-like gold (ALG) nanostructure, a sandwich-like system provided for sensitive detection of heat shock protein 70 kDa (HSP70), which applied as a functional biomarker in diagnosis/prognosis of COVID-19. Initially, the surface of the GCE was improved with rGO and ALG nanostructures, respectively. Then, an aptamer sequence as the first part of the bioreceptor was covalently bound on the surface of the GCE/rGO/ALG nanostructures. After adding the analyte, the second part of the bioreceptor (aptamer-AuNPs) was immobilized on the electrode surface to improve the diagnostic performance. The designed aptasensor detected HSP70 in a wide linear range, from 5 pg mL^{-1} to 75 ng mL^{-1}, with a limit of detection (LOD) of ~2 pg mL^{-1}. The aptasensor was stable for 3 weeks and applicable in detecting 40 real plasma samples of COVID-19 patients. The diagnostic sensitivity and specificity were 90% and 85%, respectively, compared with the reverse transcription-polymerase chain reaction (RT-PCR) method.

1. Introduction

Coronaviruses are a large group (*Coronaviridae*) of viruses that can cause some infections, from a common cold to acute respiratory challenges. So far, four types of coronaviruses have been identified (α, β, γ, and δ) which human coronaviruses are found only in α and β groups [1]. The genomic sequencing confirmed the similarity between the recent coronavirus and two types of β-coronavirus (SARS-like and MERS-CoV) [2,3]. Hence, the new β-coronavirus was named severe acute respiratory syndrome coronavirus 2 (SARS-CoV-2) [4]. The SARS-COV-2

* Corresponding author.
** Corresponding author.
E-mail addresses: mnegahdary@iq.usp.br (M. Negahdary), luangnes@iq.usp.br (L. Angnes).

https://doi.org/10.1016/j.aca.2022.340716
Received 1 November 2022; Accepted 7 December 2022
Available online 8 December 2022

transmitted disease was named COVID-19 by the World Health Organization (WHO) [5]. Unfortunately, from the beginning of its emergence until November 2022, it has led to 635 million definitive infections and ~6.6 million deaths worldwide [6]. The United States, India, Brazil, France, and Germany have had the highest number of diagnosed true-positive (TP) cases [6]. Till now, Different methods have been used to diagnose this disease, including designing/applying complementary RNA sequences of the virus genome, antigens, and antibodies related to this virus [7]. The most important method of diagnosing COVID-19 in clinics and hospitals is the real-time reverse transcription-polymerase chain reaction (RT-PCR) [8].

Patients' samples for diagnosing this disease mainly include important biofluids (blood, saliva, and nasopharyngeal swab) [9]. HSP70 is one of the critical biomarkers with great potential for the diagnosis/prognosis of COVID-19. Heat shock proteins (HSPs) are a set of proteins found in all living organisms and are classified according to their molecular weight, and the major ones include HSP27, HSP40, HSP60, HSP70, HSP90, and HSP110 [10]. The transcription process related to the production of these proteins increases or decreases in response to temperature shocks, stress, harmful chemicals, metabolic instabilities, and hypoxia/anoxia that facilitate folding and maintaining cellular protein structure [11]. The most important heat shock protein is HSP70, which has been shown to have varying levels of concentration in COVID-19 [12], cancer [13], diabetes [14], and some heart diseases [15]. So it can be used as a diagnostic biomarker. In a clinical study, the concentrations of HSP70 in the plasma of COVID-19 patients admitted to the intensive care unit (ICU) were evaluated. The increased HSP70 levels were confirmed as a biomarker predicting mortality for COVID-19 patients [12]. This biomarker was reported at a relatively stable level of 200 ng mL^{-1} during a one-week evaluation. Also, in one of the other recent studies, it has been shown that this biomarkers' maximum level in healthy individuals' plasma is about 35 ng mL^{-1} [16].

Aptasensors as innovative detection tools are a subset of biosensors introduced in 1990 [17]. These quantitative diagnostic systems are extensively designed to diagnose various diseases [18–20]. In aptasensors, short single-stranded DNA or RNA sequences are used as the bioreceptor that is purposefully designed and can be specifically attached to target molecules [21]. Optimizing aptasensor components such as the bioreceptor and the signal transducer with various nanomaterials has recently been widely pursued [22]. Nanomaterials often amplify the aptasensors diagnostic signal and increase their sensitivity [23]. Moreover, nanomaterials can improve the stability of aptasensors [24]. Among the nanomaterials, carbon-based nanomaterials and nanomaterials synthesized from gold have received the greatest attention. GO is a carbon-based nanomaterial that comprises two-dimensional (2D) biocompatible graphene plates containing oxygen groups like hydroxyl and epoxide on its surfaces [25,26]. The presence of the mentioned functional groups reduces the conductivity of GO, and therefore by eliminating/minimizing these groups, GO in its reduced form (rGO) can have an outstanding performance in modifying the signal transducer surface [27–29]. On the other hand, gold-based nanomaterials have been used in the design of aptasensors due to their high conductivity, simple synthesis, high flexibility, and compatibility with biomolecules [30].

Many biosensors, such as aptasensors, immunosensors, and other types, have been designed to diagnose COVID-19 (detecting of related genes, antigens, and antibodies) [31–36]. Using these aptasensors as an alternative approach to substitute expensive and highly limited methods such as RT-PCR can play a beneficial role in controlling epidemics in the future [37]. In addition, aptasensors can reduce the false-negative (FN) and false-positive (FP) results reported by other methods. Due to the higher sensitivity of HSP70 to cell-related instabilities, this biomarker increases rapidly in COVID-19 patients and can reflect the disease more early than other introduced analytes [12,16].

Herein, an aptasensor was constructed to diagnose COVID-19 by detecting HSP70. The signal transducer was a GCE modified with a thin layer of rGO and ALG nanostructure, respectively (Fig. 1). Then, the immobilization of a thiol-functionalized aptamer was performed on the electrode surface. Subsequently, different concentrations of HSP70 were added to the surface of the GCE/rGO/ALG nanostructure/aptamer. Finally, aptamer-AuNPs was added to the electrode surface as the second part of the bioreceptor. Aptamer molecules (by changing their conformation) in a sandwich-like state could have a high affinity for capturing the analyte. In the absence of the analyte, redox agents had more access to the surface of GCE (DPV peak current: maximum value). Conversely, in the presence of the analyte, a linear association was found between the regular reducing of DPV peak currents and enhancing the analyte concentration (signal-off aptasensor). The presence of AuNPs helped to maintain the conductivity of the signal transducer for a very wide concentration range in a serial analysis of various concentrations of the analyte. This decrease in DPV peak currents was related to the limited access of the redox agent to the electrode surface due to the found electrostatic repulsion between the negatively charged aptamer strands (in the sandwich-like structure) and the redox molecules.

2. Materials and methods

2.1. Materials/reagents

HSP70, HSP90, human serum albumin (HSA), immunoglobulin G (IgG), heparin, hemoglobin (Hb), a thiol functionalized aptamer (5′–SH–C_6- GGGAGACAAGAAUAAACGCUCAAUGCGCUGAAUGCCCAG CCGUGAAAGCGUCGAUUUCCAUCCUUCGACAGGAGGCUCACAACAG GC-3′(Merck Batch number: WD09700943) [38], spermine, dithiothreitol (DTT), Tris (2-carboxyethyl) phosphine (TCEP), 6-mercapto-1--hexanol (MCH), GO, $HAuCl_4$, trisodium citrate dihydrate, ethylene diaminetetraacetic acid (EDTA), and ethanol were purchased from Millipore Sigma (USA). All other reagents and chemicals were of the highest quality commercial grades and were used without further purification.

2.2. Apparatus

Two potentiostat/galvanostat devices were used to conduct electrochemical experiments (Autolab-PGSTAT302 N and PalmSens, Netherlands). The surface of employed working electrodes was characterized by a field emission scanning electron microscope (FESEM) equipped with an energy dispersive X-ray spectrometer (EDS) (JEOL JSM 7401F, Japan). The surface of the GCE/rGO/ALG nanostructure before analysis by the FESEM was coated with a layer (3 nm) of gold performed by Cressington 208HR sputter coater (Cressington Scientific Instrument Ltd., Watford, UK). The morphology of AuNPs and aptamer-conjugated AuNPs utilized as the second part of the bioreceptor was investigated by a high-resolution transmission electron microscope (HRTEM) (JEOL JEM-2100, Japan). A UV–Vis spectrophotometer (HP 8453, Agilent Technologies., USA) was applied to confirm the proper synthesis of AuNPs and aptamer-conjugated AuNPs. In order to perform another characterization, the instrument of Malvern Zetasizer equipment (Malvern Instruments Ltd., UK) equipped with Zetasizer software (version 7.11) was applied to determine the average size of AuNPs.

2.3. Synthesis of AuNPs

The AuNPs were synthesized based on the previous protocol but with some modifications [39]. First, all the required utensils and components of the reflux system were washed with aqua regia (following all the safety principles). A solution containing 50 mL of 1 mmol L^{-1} $HAuCl_4$ (dissolved in the deionized water (DI water) water with the desired quality (resistivity = 18.2 MΩ cm)) was prepared, transferred to the reflux system and heated until boiling. Afterward, 5 mL of 66 mmol L^{-1} trisodium citrate dehydrate was injected into the reflux system. After enough time, the color of the solution changed from yellow to black, in

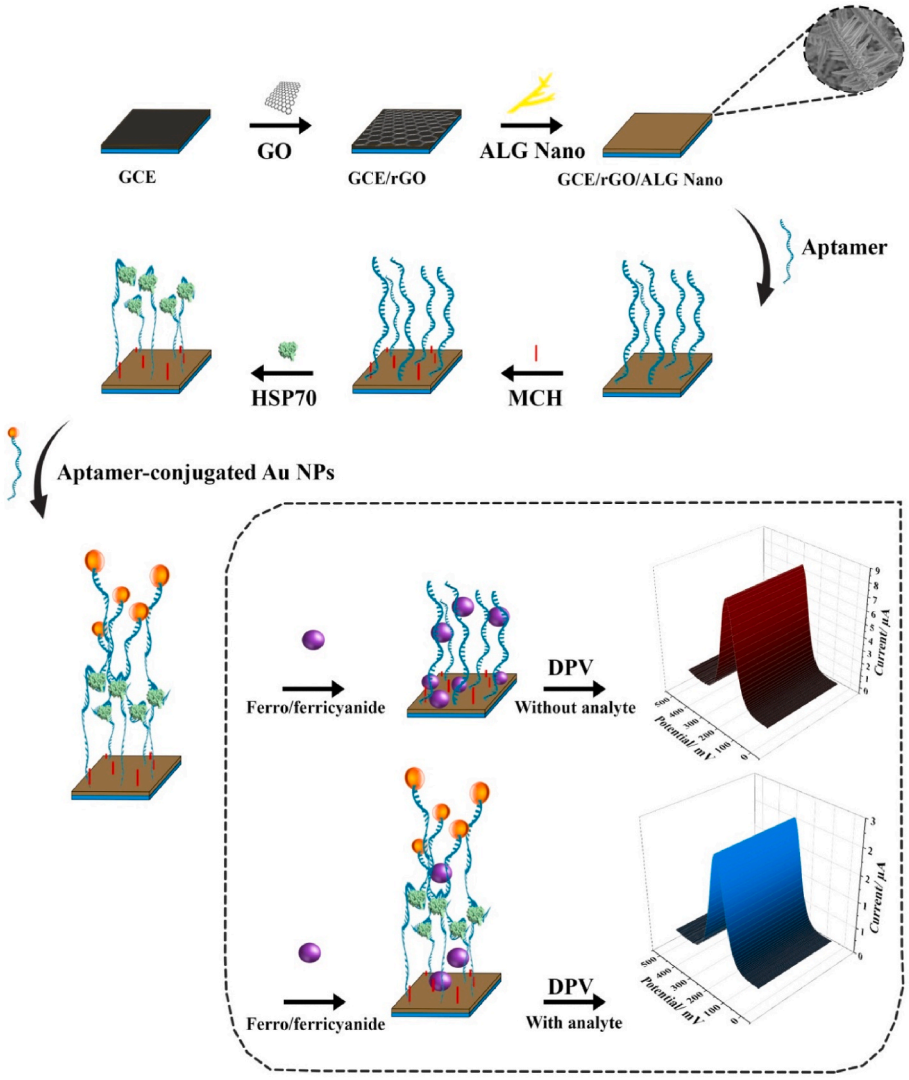

Fig. 1. Schematic presentation of the sandwich-like aptasensing platform to diagnose COVID-19 through detection of HSP70.

sequence to purple, and finally to deep red (synthesized form). Subsequently, the synthesized AuNPs were cooled at room temperature, characterized by UV–Vis spectroscopy and TEM, and stored in a dark and refrigerated (4 °C) condition until further use.

2.4. Preparing aptamer-conjugated AuNPs

The aptamer-conjugated AuNPs were synthesized based on the previously reported protocols and with some modifications [39,40]. Here, a vial containing 50 μL of 20 μmol L^{-1} thiolated HSP70 aptamer, 10 μL acetate buffer (500 mmol L^{-1}, pH 5.2), and 10 μL of 10 mmol L^{-1} TCEP was prepared and incubated at 25 °C for 120 min. Then, the vial's content was transferred to a tube containing 2 mL of the synthesized AuNPs (section 2.3) and stored in a dark place (covered by aluminum foil) for 16 h at 25 °C. Afterward, 10 μL Tris-acetate (500 mmol L^{-1}, pH 8.2) was added gradually. In another step, 150 μL of 1 mol L^{-1} NaCl was added slowly, and the achieved mixture was stored in a dark place (covered by aluminum foil) for another 16 h at room temperature. Ultimately, the mixture was centrifuged at high speed (15000 rpm) for 20 min, and then the upper layer was discarded. The synthesized aptamer-conjugated AuNPs were characterized by UV–Vis spectroscopy and TEM. The aptamer-conjugated AuNPs were stored in a dark and refrigerated (4 °C) until further use.

2.5. Preparing of HSP70 aptasensor

For electrochemical experiments, a three-electrode system was used. The working, counter, and reference electrodes were GCE (2 mm ⌀, Metrohm, Netherlands), a platinum wire, and an Ag/AgCl, 3 mol L^{-1} KCl (Metrohm, Netherlands), respectively. Initially, the working electrode was polished on an alumina (0.3 μm) polishing pad to a mirror finish and then cleaned in ethanol/DI water (3:1) using an ultrasonic bath for 8 min. In the next step, the electrode was electrochemically cleaned by cyclic voltammetry (CV) in the presence of 0.5 mol L^{-1} H_2SO_4 (procedure detail: scan rate: 50 mV S^{-1}, potential range: -1 to 1 V, and 20 continuous cycles). Afterward, the electrode was immersed in the 500 μg mL^{-1} GO solution. Nitrogen was injected into the synthesis solution, and the electrodeposition process was performed by the chronoamperometry method (potential: -1.5 V, time: 400 s). This procedure reduced a 2D layer of GO sheets on the surface of GCE. Then, the modified GCE/rGO was immersed in the synthesis solution of the ALG nanostructure (15 mmol L^{-1} $HAuCl_4$, 500 mmol L^{-1} H_2SO_4, and 50 mmol L^{-1} spermine), and the second surface modification was done by the chronoamperometry method (potential: 200 mV, time: 250 s). Since the applied aptamer was thiol-functionalized, in order to break thiol molecules and provide a reduced form of the aptamer, 20 μL of a solution (500 mmol L^{-1} DTT and 10 mmol L^{-1} sodium acetate (pH 5.2)) was added to 20 μL of the optimized concentration of aptamer (detailed in

section 2.6). After keeping the aptamer vial for 20 min at room temperature, the DTT was extracted by adding 3 times ethyl acetate (each time: 100 μL), vortexing, and discarding the upper layer. Then, the surface of the GCE/rGO/ALG nanostructure was covered with the activated aptamer, and the immobilization process was processed in refrigerated condition (4 °C). The thiol group of aptamer established the covalent bond (Au–S) with the gold associated with the ALG nanostructure. Considering the time for covalently attachment of the aptamer on the surface (detailed in section 2.6), the GCE/rGO/ALG nanostructure/aptamer was covered with 1 mmol L^{-1} MCH (30 min) to block unwanted/unspecific immobilization of aptamer molecules on the surface of GCE/rGO/ALG nanostructure. Subsequently, 10 μL of HSP70 (various concentrations from 5 pg mL^{-1} to 75 ng mL^{-1}) was dropped on the surface of the electrode, and then 10 μL of the prepared aptamer-conjugated AuNPs (section 2.4) was added. After considering enough binding time (detailed in section 2.6) at 37 °C, the electrochemical assays were achieved using the differential pulse voltammetry (DPV) in the presence of the redox electrolyte (20 mM Tris-HCl buffer, 500 mmol L^{-1} KCl, 0.5 mmol L^{-1} $K_4[Fe(CN)_6]/K_3[Fe(CN)_6]$).

2.6. Optimizing the aptamer condition

Open circuit potential (OCP) analysis was performed to find the best required time for immobilizing of aptamer on the surface of the working electrode. This experiment was performed in the presence of several screen-printed carbon electrodes (SPCE) (110, Metrohm DropSens, Spain). Due to the necessity of using refrigerated conditions to minimize environmental contamination and preventing the aptamer from drying on the surface, as well as the facility to use the smallest volume of aptamer, this experiment was performed using the SPCE instead of GCE. So, after preparing SPCE/rGO/ALG nanostructure, different concentrations (2, 5, 10, 15, 25, and 50 μmol L^{-1}) of aptamer were immobilized separately and in a refrigerated condition (4 °C). Potential changes were recorded for 12 h. The best time required for aptamer immobilization on the electrode surface was obtained by considering the first time corresponding to the first potential steadying point. In another experiment, the GCE/rGO/ALG nanostructure was prepared, and different concentrations (2, 5, 10, 15, 25, and 50 μmol L^{-1}) of aptamer were immobilized on its surface. Following MCH treatment, a DPV was recorded for each aptamer concentration. The concentration corresponding to the first steady peak DPV currents was utilized in all future assays as the desired aptamer concentration. After finding the desired aptamer concentration and aptamer immobilization time, a typical concentration (1 ng mL^{-1}) of analyte was dropped on the surface of the GCE/rGO/ALG nanostructure/aptamer. Then aptamer-AuNPs were added, and GCE/rGO/ALG nanostructure/aptamer/HSP70/aptamer-AuNPs were obtained. This aptasensor was placed in an incubator (37 °C), and a DPV was recorded every 4 min; when the first steady point in the DPVs peak current was attained, the desired binding time related to the interaction between aptamer strands and analyte was identified. Therefore, in all subsequent experiments, the found binding time was used.

2.7. Evaluation criteria for the reproducibility, regeneration, and stability assays

In order to determine the reproducibility, the aptasensor bound with a typical concentration of analyte (GCE/rGO/ALG nanostructure/aptamer/HSP70 (1 ng mL^{-1})/aptamer-AuNPs) was refabricated seven times, and then related DPVs were recorded. After each time, the aptasensor was soaked in piranha solution for 1 min to eliminate all organic molecules from the surface of the signal transducer. After washing with the DI water, the obtained electrode (GCE/rGO/ALG nanostructure) was applied for the next aptasensor refabricating. For the regeneration monitoring, the aptasensor was bound with HSP70 (1 ng mL^{-1}), and debound (by immersing in hot (95 °C) DI water for 5 min [41,42]), and related DPVs were recorded for both statuses. The mentioned assay was repeated seven times. To assess stability, the constructed aptasensor was bound with HSP70 (1 ng mL^{-1}), and the corresponding DPV was recorded for a continuous period (10 times DPV recording for 21 days). After each DPV recording, the electrode was rinsed with DI water and refrigerated in Tris-HCl buffer (pH 7.4).

2.8. Evaluation criteria for specificity analysis

Several biomolecules (HSP90, Hb, heparin, HSA, and IgG) were used as interfering agents to investigate the specificity performance of the developed aptasensor. In addition, mixtures of all mentioned interfering agents and the analyte were considered as another interfering group. In these groups, a concentration (1 ng mL^{-1}) of the analyte was used in the presence of three concentrations (1 ng mL^{-1}, 10 ng mL^{-1}, and 1 μg mL^{-1}) of HSP90 and three concentrations (10 ng mL^{-1}, 1 μg mL^{-1}, and 100 μg mL^{-1}) of other interferences. Nevertheless, for the aptasensor performance in the presence of interferences mixtures, the concentrations of HSP70 were 1 ng mL^{-1} and 100 ng mL^{-1}, and concentrations related to mixtures of all interferences were 100 ng mL^{-1} and 100 μg mL^{-1}. DPVs were recorded, and the maximum peak decrement in each group was considered 100%, and the decrement percentages for other agents were obtained compared to 100%.

2.9. COVID-19 real samples applying criteria and ethics

This research was permitted by the research ethics committee of BP-A Beneficência Portuguesa de São Paulo hospital (CAAE number 36730020.6.0000.5483). All patients or their legal representatives provided informed consent. The study included 40 patients of both genders, older than 18-year-old and diagnosed with COVID-19 by RT-PCR attended at Hospital BP-A Beneficência Portuguesa de São Paulo. All patients were hospitalized no longer than 5 days at the time of inclusion, were followed up during hospitalization, and were evaluated by clinicians. Each patient's electronic medical records were inspected for demographic, clinical, and laboratory information. Plasma samples were obtained from blood collected in EDTA tubes on the day of inclusion and the day of hospital discharge. The plasma samples categorized into two groups (each group: 20 samples) were considered for assessment. Group 1 was related to samples detected before as COVID-19 positive by the RT-PCR method, and these patients were hospitalized based on the RT-PCR result and clinical symptoms. The second group (group 2) contained samples related to the same patients at the time of recovery and their discharge from the hospital. The electrochemical assay for plasma samples was done in a lab with certified biosafety control in the Pharmacy Sciences Faculty from the University of São Paulo (USP). Before electrochemical measurements, plasma samples were diluted 10 times with normal saline solution (0.9% NaCl). Every 5 pairs of samples (5 samples related to the first day (group 1) and 5 samples related to the discharge day (group 2)) were evaluated electrochemically in one day. The DPV peak current of plasma samples was compared with the DPV peak current related to the standard HSP70. The DPV peak current was used to estimate the concentration of HSP70 in the plasma of COVID-19 patients. For group 1, the results related to the RT-PCR method were considered as the reference. Moreover, true-positive (TP), true-negative (TN), FP, and FN results by considering the cut-off value (35 ng mL^{-1} [16]) of HSP70 in the plasma of healthy individuals were determined to find the diagnostic sensitivity and diagnostic specificity of the designed aptasensor. It should be considered that all samples related to the discharge day (group 2) from the hospital were assumed as TN.

2.10. Analysis of data

The data relating to electrochemical analyses were provided by Nova (version 1.11) and PSTrace (version 5.7) software. Analyses of electrochemical data and UV–Vis spectroscopy were performed via Microsoft

Excel (version 2010) and Origin (version 2019). Image analysis related to SEM and TEM results were followed by Digimizer (version 4.5.2).

3. Results and discussion

3.1. Characterization of the modified GCE with GO and ALG nanostructure

The surface of a GCE was modified with GO and ALG nanostructure through the electrodeposition method, and then modified surfaces were characterized by the FESEM. The time and applied potential during the electrodeposition process were effective in the morphology of produced materials. For modifying the surface of GCE (Fig. 2-a) with the reduced GO (rGO), the optimized condition was potential: -1.5 V and time: 400 s (Figs. S1–a and Fig. 2-b). The presence of 2D sheets of rGO on the surface of GCE enhanced the reactivity and electrocatalytic behavior of the signal transducer explained in section 3.3 with comprehensive detail. Optimizing the electrodeposition time related to the gold solution (section 2.5) was followed in the absence of GO. It was found that when different electrodeposition times were applied, a dissimilar layer of gold was shaped (Fig. 2-c and 2-d, electrodeposition time: 400 s) and (Fig. 2-e and 2-f, electrodeposition time: 250 s). It seems that the time and the applied potential (0.2 V) changed the interaction of spermine molecules with other reagents present in the solution. A more homogeneous distribution of synthesized shapes of the gold structure and smaller sizes of shapes was found for optimized conditions (Fig. 2-e and 2-f). Once more, GCE/rGO was prepared, and by applying the optimized condition (potential: 0.2 V, time: 250 s), it was modified with a layer of ALG nanostructure (Figs. S1–b and Fig. 2-g and 2-h). The presence of reduced graphene oxide on the surface of GCE made it possible to grow the gold structure in smaller sizes and nanometer dimensions, which provided the desired substrate for the subsequent stages. The EDS analysis also confirmed the excellent purity of the synthesized ALG nanostructure (Figs. S1–c). Considering the formal potentials based on the two principal gold redox processes ($Au^{3+} + 3e^- \rightleftharpoons Au$ and $AuCl_4^- + 3e^- \rightleftharpoons Au + 4Cl^-$, $E^0 = 1.27$ V, vs. AgCl), the applied electrodeposition potential (0.2 V) was negative [43]. The presence of spermine in the gold nanostructure solution led to the creation of electrostatic interaction with $AuCl_4^-$, which triggered the shift of gold reduction potential and the deposition of gold nanostructure on the electrode surface. We have also shadowed the use of other biogenic amines in synthesizing several other gold nanostructures in previous research [18,44]. The FESEM analysis showed that the typical arm diameter in the ALG nanostructure was about 75–100 nm (Fig. 2-g and 2-h).

3.2. Analysis of synthesized AuNPs and aptamer-conjugated AuNPs

In another experiment, the synthesized AuNPs and aptamer-conjugated AuNPs were analyzed. The average size of the generated AuNPs was confirmed by zetasizer analysis, which was about 26 nm. Afterward, aptamer-conjugated AuNPs were prepared, and then UV–Vis spectroscopy and TEM were performed to know the difference between this conjugated form and AuNPs. The visible absorbance wavelength for AuNPs was found at ~520 nm and confirmed the controlled synthesis (Fig. 2-i). Afterward, UV–Vis spectroscopy was also performed for aptamer-conjugated AuNPs. The absorbance signal decreased when the aptamer strands were conjugated with the AuNPs, indicating the contribution of aptamers to the decrease of visible light and a small shift (~523 nm). The applied aptamer was thiol-functionalized, and TEM analysis for aptamer-conjugated AuNPs confirmed that there wasn't any significant change in the size of AuNPs compared to the non-conjugated form (Fig. 2-j and 2-k). However, the important thing that can be

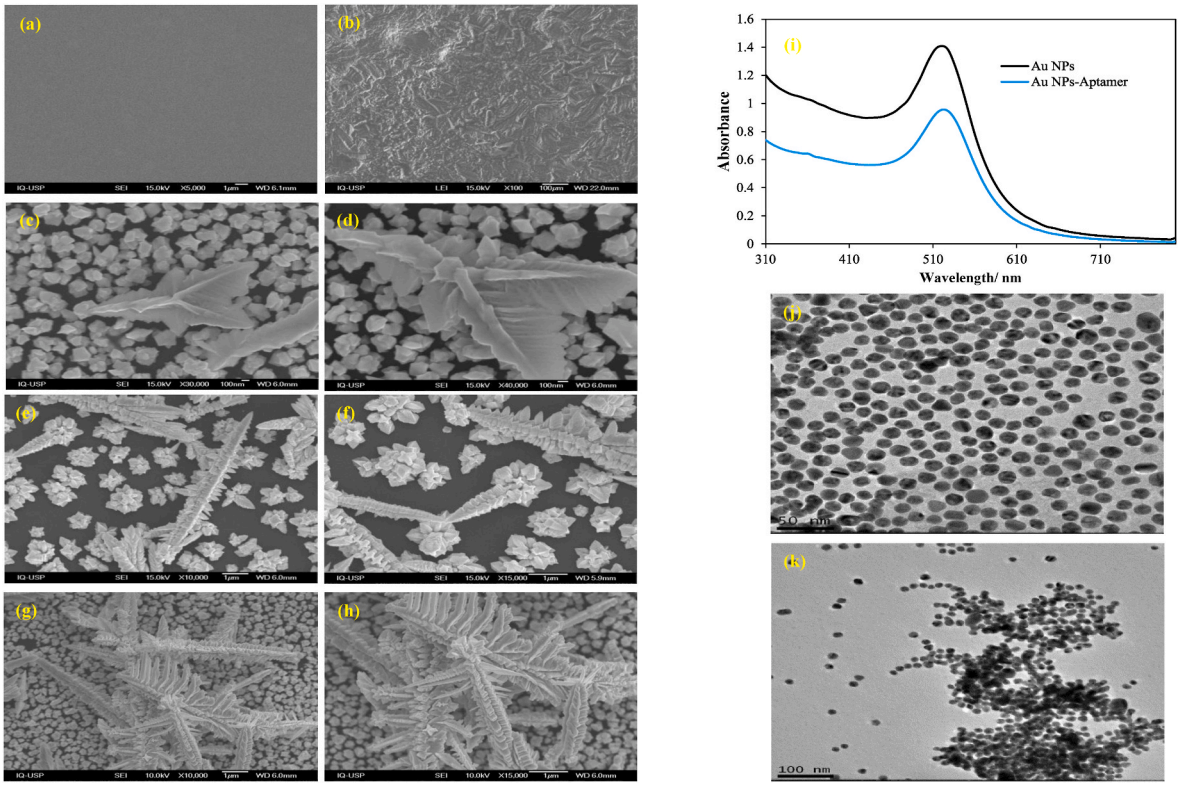

Fig. 2. FESEM micrographs of GCE (a), GCE/rGO (b), GCE/Gold nanostructure: electrodeposition time: 400 S, magnification 30 K (c), GCE/Gold nanostructure: electrodeposition time: 400 S, magnification 40 K (d), GCE/Gold nanostructure: electrodeposition time: 250 S, magnification 10 K (e), GCE/Gold nanostructure: electrodeposition time: 250 S, magnification 15 K (f), GCE/rGO/ALG nanostructure: electrodeposition time: 250 S, magnification 10 K (g), GCE/rGO/ALG nanostructure: deposition time: 250 S, magnification 15 K (h), UV–Vis of AuNPs and aptamer-AuNPs (i), TEM micrographs of AuNPs (j), and aptamer-AuNPs (k). (For interpretation of the references to color in this figure legend, the reader is referred to the Web version of this article.)

implied from the TEM images is that the presence of aptamer strands played a role in creating the network structure of nanoparticles, and the pattern of randomly dispersed AuNPs changed. This phenomenon was also confirmed in other research [45,46]. The conjugation and accumulation process changed the regular distribution of AuNPs, and most of the AuNPs were conjugated with aptamer strands.

3.3. Electrochemical analysis of GCE surface

Primarily, the signal transducer in various statuses, including GCE, GCE/rGO, and GCE/rGO/ALG nanostructure, was evaluated by CV analysis. The applied scan rates were from 2 to 200 mV s^{-1}, and CVs were recorded in the presence of 20 mM Tris-HCl buffer, 500 mmol L^{-1} KCl, 0.5 mmol L^{-1} $K_4[Fe(CN)_6]/K_3[Fe(CN)_6]$ as the redox marker (Figures S2-a, b, and c). The optimal concentrations required for GO and ALG nanostructure electrodeposition on the electrode surface were determined using this experiment so that the concentrations corresponding to the highest increase in CVs peaks compared to the bare electrode were desired (500 μg mL^{-1} GO and 15 mmol L^{-1} $HAuCl_4$). In addition, CVs in the maximum scan rate applied (200 mV S^{-1}) were shown in Fig. 3-a. The results confirmed the improvement of electron transfer rate for GCE/rGO and GCE/rGO/ALG nanostructure compared to the bare GCE. Afterward, the electrochemically active surface related to the signal transducer in various mentioned statuses was determined through the Randles-Sevcik equation ($Ip = 2.69 \times 10^5\ A \times D^{1/2}\ n^{3/2}\ v^{1/2}\ C$) [47,48]. The results (Figures S2-d and e) showed that the electrochemically active surface for bare GCE, GCE/rGO, and GCE/rGO/ALG nanostructure was 0.054, 0.066, and 0.13 cm^2, respectively. Findings confirmed that GCE/rGO electrochemically active surface was improved but only 1.22 times enhanced compared to the bare GCE. The rate for conductivity improvement based on electrochemically active surface related to GCE/rGO/ALG nanostructure compared to GCE/rGO and bare GCE was more significant, 1.97 and 2.4 times, respectively.

In another analysis, the charge transfer resistance (Rct) related to the signal transducer in various statuses was investigated by electrochemical impedance spectroscopy (EIS) (Fig. 3-b). This experiment showed excellent convergence of results and confirmed that the optimum circuit could be R([RW]Q), as depicted in Fig. 3-b. The maximum Rct was found for bare GCE (Fig. 3-b: diagram a). After modifying the surface with GO and ALG nanostructure, the Rct was decreased (Fig. 3-b: diagram b: GCE/rGO, diagram c: GCE/rGO/ALG nanostructure)). Then, the thiol-functionalized aptamer was immobilized (aptamer concentration: 15 μmol L^{-1} (Figs. S3–a), aptamer immobilization time: 130 min; (Figs. S3–b)) on the surface of the GCE/rGO/ALG nanostructure and could create Au–S covalent bound. This event led to a slight enhancement of the Rct due to electrostatic repulsion provided by the negatively charged phosphate backbone of aptamer induced to the anionic $[Fe(CN)_6]^{3-/4-}$ (Fig. 3-b: diagram d). Then, HSP70 (1 ng mL^{-1}) was dropped on the surface to be trapped by the aptamer strands from one side. Then the other part of the bioreceptor (aptamer-AuNPs) was dropped and captured the HSP70 from the other side (aptamer binding time: 24 min at 37 °C, (Fig. S4)). The reported isoelectric pH of HSP70 is about 5.4 [49]. So, the used pH by aptasensor components (pH ~ 7) and HSP70 was negatively charged and showed a more hindering electron effect on $[Fe(CN)_6]^{3-/4-}$. Thus, the interaction of the analyte with aptamer strands increased the Rct value by restricting the access of the redox molecules to the working electrode and blocking the electron transfer on the surface (Fig. 3-b: diagram e). The presence of AuNPs helped maintain the conductivity for a wider concentration range in a serial analysis of various analyte concentrations, confirmed in section 3.4.

In another analysis, the signal transducer in various statuses was evaluated by the DPV. As shown in Fig. 3-c, the lowest DPV peak current (lowest electron transfer rate) was found for the bare GCE. By modifying the surface with GO and ALG nanostructure, the DPV peak current was enhanced, and this event confirmed the enhanced surface area for interaction with the redox marker molecules.

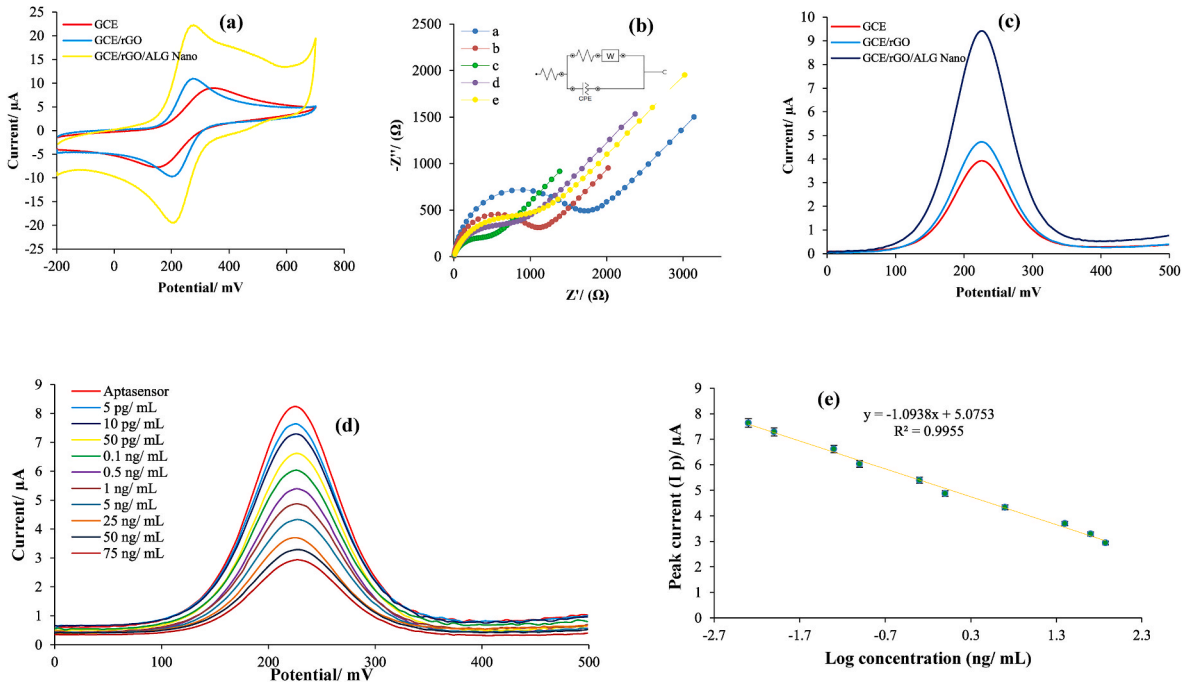

Fig. 3. CVs related to the various states of the signal transducer (scan rate: 200 mV S^{-1}) (a); EIS analysis of the various states of the signal transducer: a) GCE, b) GCE/rGO, c) GCE/rGO/ALG nanostructure, d) GCE/rGO/ALG nanostructure/aptamer (without analyte), e) GCE/rGO/ALG nanostructure/aptamer/HSP70 (1 ng mL^{-1})/aptamer-AuNPs; DPVs of the various states of the signal transducer (c); DPVs (signal-off) of aptasensor in the presence of various concentrations of HSP70 (d); calibration curve of HSP70 aptasensor (Ip vs. logarithm of analyte concentrations) (e); Error bars indicate standard deviations from three repeated measurements (error bar: SD/n = 3).

3.4. Determination of analyte concentrations

In this experiment, the constructed aptasensor was used to measure various concentrations of HSP70. The analyte was detected by the designed aptasensor throughout a wide linear range of 5 pg mL^{-1} to 75 ng mL^{-1} (concentration span: 15,000 times). By incrementing the analyte concentration, the DPVs peak current was decreased regularly (signal-off) Fig. 3- d. Here, using a sandwich-like structure in analyte detection led to an increase in diagnostic stability and maintaining the electrode conductivity at high analyte concentrations, which provided a wide range of detection for a set of analyte concentrations. In fact, the binding of aptamer-conjugated AuNPs from the other side to analyte molecules caused a slight decrease in the electron transfer process with increasing analyte concentration. Compared to the previous aptasensor designed by our team to detect this protein, in that aptasensor, the sandwich-like structure equipped with aptamer-conjugated AuNPs was not used, and the LOD and detection range was equal to 20 pg mL^{-1} and 50 pg mL^{-1} - 75 ng mL^{-1}, respectively [44], which confirms that the special design and Sandwich like aptasensor in this research has provided a more sensitive detection, with a wider and more stable range (LOD: 2 pg mL^{-1} and detection range: 5 pg mL^{-1} - 75 ng mL^{-1}). This wide detection range and possibility for a regular and stable detection response can be translated as improving the role of the present sandwich-like aptasensing platform in improving the conductivity offered by AuNPs in the conjugated form. Consequently, by considering the value of this biomarker in healthy individuals (35 ng mL^{-1}), this aptasensor can be used at upper and lower levels than the cut-off value [12,16]. Here, the elevated concentration of HSP70 was considered for monitoring hospitalized COVID-19 patients. In many reports, the level of HSP70 changes in biofluids along with the severity of several diseases. Changes in the level of HSP70 can be used to diagnose/prognosis in some other diseases, such as diabetes [14,50], cancer [13,51], heart diseases [52,53], and neurodegenerative disease [54,55]. Fig. 3-e shows the calibration curve related to various concentrations of analyte (where X = logarithm of concentrations and Y = DPVs peak current). The linear regression was: Δcurrent (μA) = −1.094 log C HSP70 + 5.075, R^2 = 0.9955. The calculated limit of detection (LOD) was about 2 pg mL^{-1} considering 3 σ (σ is the standard deviation (SD) of 10 assays of the blank signal) (S/N = 3). In Table 1, the key characteristics of the designed HSP70 biosensing platforms developed are compared with the ones that emerged in this research.

As shown in Table 1, compared to all the biosensors designed to detect HSP70 protein, none of the previous research has specifically investigated the use of HSP70 biosensing to detect real samples related to a specific disease. The HSP70 biosensor designed in this research is the first and only HSP70 biosensing platform employed in the diagnosis of real samples of a disease (plasma of Covid-19 patients). Also, compared to other designed biosensors, the highest stability (remaining

Table 1
Essential details of developed biosensors for monitoring of HSP70.

Type of biosensing	Working electrode or transducer	Bioreceptor	Nano-advanced materials	Measuring method	Linear range of detection	LOD	Stability	Human sample analysis	Application	Reference
Immunosensor (electrochemistry-based)	GCE	Anti-HSP70 antibody	Polyaniline functionalized graphene quantum dots	DPV	97.6 pg mL^{-1} - 100 ng mL^{-1}	50 pg mL^{-1}	90.16%, 15 days	Serum	-[a]	[56]
Immunosensor (electrochemistry-based)	GCE	Anti-HSP70 antibody	Porous graphene (PG)	DPV	44.8 pg mL^{-1} - 100 ng mL^{-1}	20 pg mL^{-1}	92.36%, 15 days	Serum	–	[57]
Immunosensor (electrochemistry-based)	GCE	Anti-HSP70 antibody	GO	EIS/CV	12 - 144 fg mL^{-1}	0.765 fg mL^{-1}	-♣	Serum	–	[58]
Immunosensor (electrochemistry-based)	GCE	Anti-HSP70 antibody	Fullerene C60 NPs	EIS	0.8–12.8 pg mL^{-1}	0.273 pg mL^{-1}	–	Serum	–	[59]
Immunosensor (electrochemistry-based)	Plastic chip electrode	Anti-HSP70 antibody	Au nanolayer	DPV	10 pg mL^{-1} - 1000 ng mL^{-1}	3.5 pg mL^{-1}	94.5%, 21 days	Serum	–	[60]
Immunosensor (electrochemistry-based)	Indium tin oxide electrode	Anti-HSP70 antibody	AuNPs	EIS/CV	1 - 166 fg mL^{-1}	0.0618 fg mL^{-1}	92.29%, 15 days	Serum	–	[61]
Immunosensor (electrochemistry-based)	Titanium foil	Anti-HSP70 antibody	Titanium dioxide nanotubes/Ag NPs	EIS/CV	100 pg mL^{-1} - 100 ng mL^{-1}	480 pg mL^{-1}	–	–	–	[62]
Immunosensor (optical-based)	oxidized porous silicon	Anti-HSP70 antibody	Porous silicon	UV–Vis	3–500 μg mL^{-1}	1290 ng mL^{-1}	–	–	–	[63]
Immunosensor (localized surface plasmon resonance-based)	Glass substrate	Anti-HSP70 antibody	AuNPs	LSPR	920 pg mL^{-1} - 4 μg mL^{-1}	920 pg mL^{-1}	–	–	–	[64]
Peptisensor (electrochemistry-based)	GE	Peptide	-♠	Square wave voltammetry (SWV)	0.2–2 nU mL^{-1}	–	–	–	–	[65]
Aptasensor (electrochemistry-based)	GE	Aptamer	Lady fern-like gold nanostructure	DPV	50 pg mL^{-1} - 75 ng mL^{-1}	20 pg mL^{-1}	92%, 18 days	Serum	–	[44]
Aptasensor (electrochemistry-based)	GCE	Aptamer	AuNPs/rGO/ALG nanostructure	DPV	5 pg mL^{-1} - 75 ng mL^{-1}	2 pg mL^{-1}	96.9%, 21 days	Plasma	COVID-19	This work

[a] Application for any disease monitoring not reported; ♣ Stability not reported; ♠ Nanomaterial (s) not reported.

96.9% of initial activity after 21 days) has been reported in this research, which can be related to the special structure of using different nanomaterials as well as sandwich-like aptasensing platform for detection of the analyte. Also, very low LOD and wide detection range are other important competitive advantages over other biosensors designed for HSP70.

3.5. Reproducibility, regeneration, and stability performance

In another analysis, the aptasensor bound with HSP70 (1 ng mL^{-1}) was refabricated seven times according to the criteria presented before (section 2.7). This experiment verified an excellent performance, and very low DPV peak current changes were found (RSD: 1.6%) (Fig. 4-a). In another experiment, the response of the constructed aptasensor was examined seven times after capturing a typical concentration of the analyte (1 ng mL^{-1}). After recording DPV for each bound time, the electrode was immersed in 95 °C DI water (for 5 min) to change the aptamer conformational and release the analyte molecules. So, after debinding the aptasensor from the analyte, another DPV was recorded (Fig. S5). The regeneration performance for bound and de-bound DPVs was evaluated, and the RSD for bound and de-bound DPVs was calculated as 1.11% and 1.28%, respectively, which confirmed an excellent regeneration performance. In order to determine the stability, a specific concentration (1 ng mL^{-1}) of the analyte was bound to the aptasensor, and the electrochemical performance was monitored for 21 days without any change in the structure of the aptasensor (ten DPV recorded) (Fig. 4-b). The stability of the presented aptasensor was excellent compared to other HSP70 biosensors (Table 1). After 21 days, this aptasensor could maintain 96.9% of its initial activity (RSD: 3.1%).

3.6. Specificity performance

To verify the specificity of the developed aptasensor, several interfering agents (HSP90, heparin, IgG, Hb, and HSA) were used in the presence of the analyte. The samples were prepared (detail presented in section 2.8). The DPVs related to interfering agents were achieved (Figure S6, (a-g)), and the corresponding peak current was evaluated. There was also a group containing mixtures of all interfering species and the analyte aiming to evaluate the aptasensor specificity performance. To do this experiment, a series of six groups were considered. For each series, the maximum peak decrement value (compared to the peak current of the aptasensor (blank signal)) in each group was considered 100%. The percentage values related to the presence of interfering species in each group were calculated (Fig. 4-c). The maximum interference effect was related to 100 μg mL^{-1} HSA (16.4%) compared to 1 ng mL^{-1} HSP70 (100%). The minimum interference effect was related to 10 ng mL^{-1} heparin (0.1%) compared to 1 ng mL^{-1} HSP70 (100%). So, the results showed selective aptasensing to detect HSP70, even in employing higher concentrations of the interfering agents than the analyte. This experiment confirmed that this aptasensor could be used in biofluids containing other proteins or biomolecules with the highest selectivity for detecting HSP70.

3.7. Application for diagnosis of COVID-19 patients

Forty plasma samples related to COVID-19 patients were analyzed. These samples were categorized into two groups; the group 1 samples were previously analyzed by the RT-PCR method (section 2.9). Group 2 contained samples of the same patients related to the discharge day from the hospital that was assumed as TN. Samples were diluted ten times and then assessed by the aptasensor. For each sample, a DPV was recorded (Figure S7-a, b, c, and d), and using the equation (Δcurrent (μA) = −1.094 log C HSP70 + 5.075) related to the calibration curve of standard samples (Fig. 3, (e)), concentrations associated with each DPV peak current were estimated. Considering that the samples were diluted ten times, the estimated final concentration was multiplied by ten (Table 2). Based on the reported healthy cut-off value (35 ng mL^{-1}) [12,16], two false-negative and three false-positive results were found. So, the

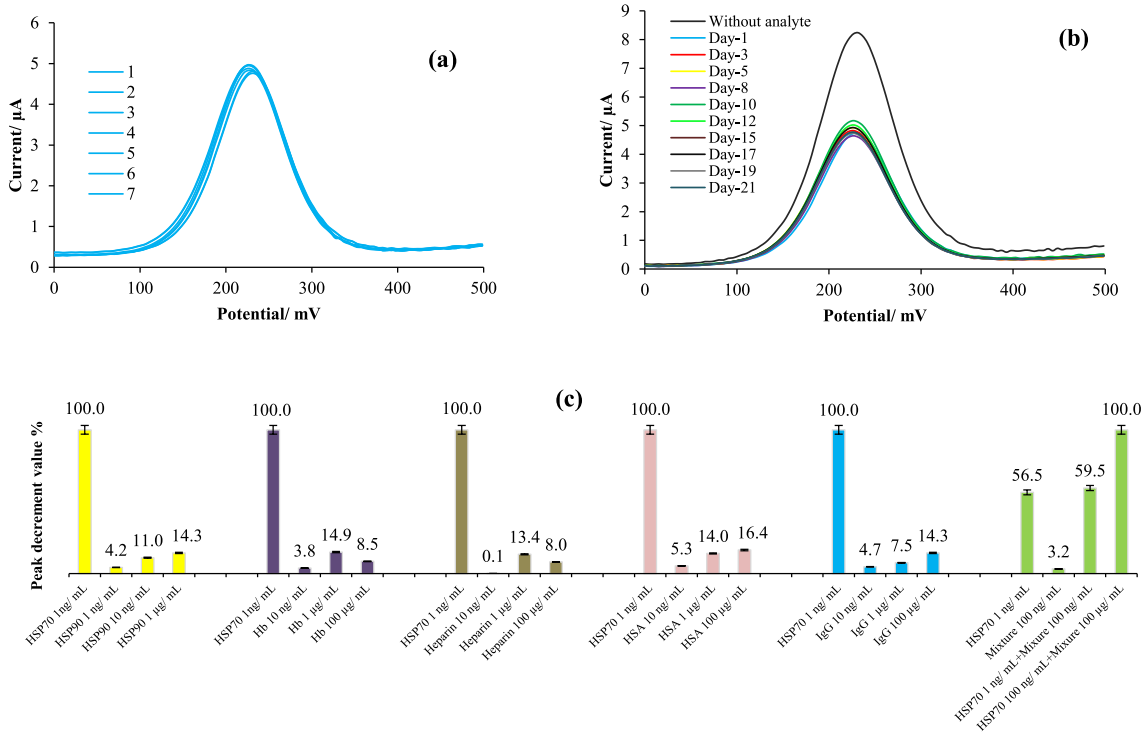

Fig. 4. Reproducibility performance for seven consecutive repeated refabricating of aptasensor (a); stability of aptasensor for 21 days analysis (b); specificity analysis of aptasensor in the presence of HSP90, Hb, heparin, HSA, IgG, and mixtures of all interfering agents; Error bars indicate standard deviations from three repeated measurements (error bar: SD/n = 3).

Table 2
Compare the performance of the designed aptasensor with the RT-PCR method in the analysis of COVID-19 patients.

Sample name	RT-PCR result	Aptasensor result	Peak current (Ip) found by aptasensor after 10 times dilution	Estimated concentration of HSP70 by aptasensor
Group 1				
S-1	Positive	Positive	3.79	116.33
S-2	Positive	Positive	3.87	98.63
S-3	Positive	Positive	3.84	103.76
S-4	Positive	Positive	3.89	94.25
S-5	Positive	Positive	3.88	97.30
S-6	Positive	Positive	3.89	95.24
S-7	Positive	Positive	3.86	101.20
S-8	Positive	Positive	3.75	125.40
S-9	Positive	Positive	3.85	102.31
S-10	Positive	Negative[a]	5.21	6.78
S-11	Positive	Positive	3.92	88.68
S-12	Positive	Positive	3.85	101.73
S-13	Positive	Positive	3.78	118.75
S-14	Positive	Positive	3.93	87.62
S-15	Positive	Positive	3.89	95.55
S-16	Positive	Positive	3.79	115.15
S-17	Positive	Negative	5.15	7.67
S-18	Positive	Positive	3.85	103.54
S-19	Positive	Positive	4.087	63.81
S-20	Positive	Positive	4.088	63.71
Group 2♠				
S-11	Negative	Negative	5.40	4.67
S-22	Negative	Negative	5.68	2.63
S-33	Negative	Negative	5.13	7.96
S-44	Negative	Positive♣	3.95	83.54
S-55	Negative	Negative	5.22	6.68
S-66	Negative	Negative	5.07	8.96
S-77	Negative	Negative	5.21	6.79
S-88	Negative	Negative	5.20	6.93
S-99	Negative	Negative	5.20	6.94
S-10–10	Negative	Negative	5.07	9.03
S-11–11	Negative	Positive	3.85	102.60
S-12–12	Negative	Negative	5.21	6.80
S-13–13	Negative	Negative	5.12	8.02
S-14–14	Negative	Negative	5.59	3.14
S-15–15	Negative	Positive	3.80	113.07
S-16–16	Negative	Negative	5.34	5.20
S-17–17	Negative	Negative	5.33	5.32
S-18–18	Negative	Negative	5.63	2.93
S-19–19	Negative	Negative	5.47	4.00
S-20–20	Negative	Negative	5.30	5.57

[a] False-negative; ♣ False-positive; ♠ All samples of this group were assumed as TN.

diagnostic sensitivity and the diagnostic specificity of the designed aptasensor for the diagnosis of COVID-19 patients were 90% and 85%, respectively.

4. Conclusion

In the presented study, a novel aptasensor was developed to detect COVID-19. This aptasensor could detect the HSP70, which can be used as a biomarker in the diagnosis/prognosis of COVID-19. Once the plasma level of this protein in COVID-19 patients increased sharply, the mentioned aptasensor provided a reliable diagnosis for this viral disease. Using different nanomaterials (AuNPs, ALG nanostructure, and rGO) increased the sensitivity, the linear detection range, and the stability of the desired aptasensor. Utilizing aptamer strands in two positions (directly immobilized on the surface of the working electrode and also conjugated with AuNPs) provided optimal conditions for the analyte detection. The presence of rGO sheets on the GCE distributed a specific and stable surface for the deposition of ALG nanostructure. In particular, the proficiency of the designed diagnostic platform in the assays of real plasma samples of COVID-19 patients was also evaluated. In the future, the role of the HSP70 biomarker in diagnosing other diseases, such as various cancers, heart diseases, and diabetes, should also be investigated. In addition, in the subsequent research, other nanomaterials, signal transducers, and bioreceptors (antibodies and peptides) can be considered in the presence of aptamers.

Study limitations

Despite the excellent diagnostic sensitivity and specificity of the designed aptasensor for HSP70, it is important to highlight that this protein is not specific to COVID-19 and may also be involved in other diseases. Moreover, Group 2 contained samples related to the discharge day from the hospital. However, no tests have been performed in the hospital for this group to prove COVID-19 negative results.

Declaration of competing interest

The authors declare that they have no known competing financial interests or personal relationships that could have appeared to influence the work reported in this paper.

Data availability

No data was used for the research described in the article.

Acknowledgments

The authors would like to thank the Sao Paulo Research Foundation-FAPESP (projects 2019/27021-4, 2017/13137-5, and 2014/50867-3) and the National Council for Research-CNPq (processes 311847-2018-8 and 465389/2014–7). The authors are also appreciative to Central Analítica (IQ-USP), Laboratório de Microscopia e Microanálise do Centro de Ciência e Tecnologia de Materiais do IPEN/CNEN-SP, Laboratório de Química Supramolecular e Nanotecnologia (IQ-USP), and Laboratório de Materiais Eletroativos (LME-IQ-USP) for material characterization facilities. We appreciate department of Clinical and Toxicological Analyses (FCF-USP) and also Hospital A Beneficência Portuguesa, SP for supporting and providing clinical sample analysis facilities.

Appendix A. Supplementary data

Supplementary data to this article can be found online at https://doi.org/10.1016/j.aca.2022.340716.

References

[1] T. Asselah, D. Durantel, E. Pasmant, G. Lau, R.F. Schinazi, COVID-19: discovery, diagnostics and drug development, J. Hepatol. 74 (2021) 168–184.
[2] X. Li, M. Geng, Y. Peng, L. Meng, S. Lu, Molecular immune pathogenesis and diagnosis of COVID-19, J. Pharmaceut. Anal. 10 (2020) 102–108.
[3] T.M. Abd El-Aziz, J.D. Stockand, Recent progress and challenges in drug development against COVID-19 coronavirus (SARS-CoV-2)-an update on the status, Infect. Genet. Evol. 83 (2020), 104327.
[4] F. Wu, S. Zhao, B. Yu, Y.-M. Chen, W. Wang, Z.-G. Song, Y. Hu, Z.-W. Tao, J.-H. Tian, Y.-Y. Pei, A new coronavirus associated with human respiratory disease in China, Nature 579 (2020) 265–269.
[5] I. Chakraborty, P. Maity, COVID-19 outbreak: migration, effects on society, global environment and prevention, Sci. Total Environ. 728 (2020), 138882.
[6] W.H.O. (WHO), WHO Coronavirus Disease (COVID-19) Weekly Epidemiological Update and Weekly Operational Update, 2022.
[7] S.S. Mahshid, S.E. Flynn, S. Mahshid, The potential application of electrochemical biosensors in the COVID-19 pandemic: a perspective on the rapid diagnostics of SARS-CoV-2, Biosens. Bioelectron. 176 (2021), 112905.
[8] O.S. Cirit, E. Mutlu, B. Sancak, T. Kocagöz, Ö. Can, C. Çicek, A. Arzu Sayiner, Ö. Appak, N.Y. Uyar, C. Külah, Comparison of a novel antigen detection test with reverse transcription polymerase chain reaction assay for laboratory diagnosis of SARS-CoV-2 infection, Infection (2022) 1–6.
[9] N. Shakeeb, P. Varkey, A. Ajit, Human saliva as a diagnostic specimen for early detection of inflammatory biomarkers by real-time RT-PCR, Inflammation 44 (2021) 1713–1723.

[10] R.F. Putri, T.E. Susilorini, N. Widodo, K. Kuswati, S. Suyadi, in: Heat Shock Protein (HSP) Release Mechanism under Heat Stress Pressure in Goats: a Review, E3S Web of Conferences, 2022, 00046.
[11] C.W. Yun, H.J. Kim, J.H. Lim, S.H. Lee, Heat shock proteins: agents of cancer development and therapeutic targets in anti-cancer therapy, Cells 9 (2019) 60.
[12] D.D. Fraser, G. Cepinskas, M. Slessarev, C. Martin, M. Daley, M.R. Miller, D. B. O'Gorman, S.E. Gill, E.K. Patterson, C.C. Dos Santos, Inflammation Profiling of Critically Ill Coronavirus Disease 2019 Patients, vol. 2, Critical care explorations, 2020.
[13] M.A. Vostakolaei, L. Hatami-Baroogh, G. Babaei, O. Molavi, S. Kordi, J. Abdolalizadeh, Hsp70 in cancer: a double agent in the battle between survival and death, J. Cell. Physiol. 236 (2021) 3420–3444.
[14] A.A. de Oliveira, V.O. Mendoza, S. Rastogi, K.P. Nunes, New Insights into the Role and Therapeutic Potential of HSP70 in Diabetes, Pharmacological Research, 2022, 106173.
[15] W.A. Kadhim, N.M. Kareem, S.A. Al-Shami, Comparison between HSP70 levels in acute and chronic coronary artery diseases, Indian J. Forensic Med. Toxicol. 14 (2020).
[16] C. Werner, S. Stangl, L. Salvermoser, M. Schwab, M. Shevtsov, A. Xanthopoulos, F. Wang, A.B. Dezfouli, D. Thölke, C. Ostheimer, Hsp70 in liquid biopsies—a tumor-specific biomarker for detection and response monitoring in cancer, Cancers 13 (2021) 3706.
[17] P. Lasserre, B. Balansethupathy, V.J. Vezza, A. Butterworth, A. Macdonald, E. O. Blair, L. McAteer, S. Hannah, A.C. Ward, P.A. Hoskisson, SARS-CoV-2 aptasensors based on electrochemical impedance spectroscopy and low-cost gold electrode substrates, Anal. Chem. 94 (2022) 2126–2133.
[18] M. Negahdary, M. Behjati-Ardakani, N. Sattarahmady, H. Yadegari, H. Heli, Electrochemical aptasensing of human cardiac troponin I based on an array of gold nanodumbbells-Applied to early detection of myocardial infarction, Sensor. Actuator. B Chem. 252 (2017) 62–71.
[19] M. Negahdary, Aptamers in nanostructure-based electrochemical biosensors for cardiac biomarkers and cancer biomarkers: a review, Biosens. Bioelectron. 152 (2020), 112018.
[20] M. Heiat, M. Negahdary, Sensitive diagnosis of alpha-fetoprotein by a label free nanoaptasensor designed by modified Au electrode with spindle-shaped gold nanostructure, Microchem. J. 148 (2019) 456–466.
[21] M. Negahdary, H. Heli, An ultrasensitive electrochemical aptasensor for early diagnosis of Alzheimer's disease, using a fern leaves-like gold nanostructure, Talanta 198 (2019) 510–517.
[22] S. Gopi, P. Balakrishnan, N.M. Mubarak, Nanotechnology for Biomedical Applications, Springer, 2022.
[23] M. Negahdary, L. Angnes, Electrochemical aptamer-based nanobiosensors for diagnosing Alzheimer's disease: a review, Biomater. Adv. 135 (2022), 112689.
[24] N. Zhang, J. Li, B. Liu, D. Zhang, C. Zhang, Y. Guo, X. Chu, W. Wang, H. Wang, X. Yan, Signal enhancing strategies in aptasensors for the detection of small molecular contaminants by nanomaterials and nucleic acid amplification, Talanta 236 (2022), 122866.
[25] Y. Zhao, Y. Liu, X. Zhang, W. Liao, Environmental transformation of graphene oxide in the aquatic environment, Chemosphere 262 (2021), 127885.
[26] Y. Ren, F. Yu, X.-G. Li, J. Ma, Recent progress on adsorption and membrane separation for organic contaminants on multi-dimensional graphene, Mater. Today Chem. 22 (2021), 100603.
[27] V. Milosavljevic, K. Mitrevska, V. Adam, Benefits of oxidation and size reduction of graphene/graphene oxide nanoparticles in biosensing application: classification of graphene/graphene oxide nanoparticles, Sensor. Actuator. B Chem. 353 (2022), 131122.
[28] J. Gao, C. Wang, Y. Chu, Y. Han, Y. Gao, Y. Wang, C. Wang, H. Liu, L. Han, Y. Zhang, Graphene oxide-graphene Van der Waals heterostructure transistor biosensor for SARS-CoV-2 protein detection, Talanta 240 (2022), 123197.
[29] J. Mondal, S.K. Srivastava, Room-temperature one-step synthesis of silver/reduced graphene oxide nanocomposites as an excellent microwave absorber, Langmuir 37 (2021) 13409–13419.
[30] M. Negahdary, Electrochemical aptasensors based on the gold nanostructures, Talanta 216 (2020), 120999.
[31] J. Zeng, P.A. Duarte, Y. Ma, O. Savchenko, L. Shoute, Y. Khaniani, S. Babiuk, R. Zhuo, G.N. Abdelrasoul, C. Charlton, An impedimetric biosensor for COVID-19 serology test and modification of sensor performance via dielectrophoresis force, Biosens. Bioelectron. (2022), 114476.
[32] M. De Felice, M. De Falco, D. Zappi, A. Antonacci, V. Scognamiglio, Isothermal amplification-assisted diagnostics for COVID-19, Biosens. Bioelectron. (2022), 114101.
[33] R. Funari, H. Fukuyama, A.Q. Shen, Nanoplasmonic multiplex biosensing for COVID-19 vaccines, Biosens. Bioelectron. 208 (2022), 114193.
[34] L. Huang, Y. Li, C. Luo, Y. Chen, N. Touil, H.-E. Annaz, S. Zeng, T. Dang, J. Liang, W. Hu, Novel nanostructure-coupled biosensor platform for one-step high-throughput quantification of serum neutralizing antibody after COVID-19 vaccination, Biosens. Bioelectron. 199 (2022), 113868.
[35] A.K. Paulose, C.C. Huang, P.H. Chen, A. Tripathi, P.H. Chen, Y.S. Huang, Y. L. Wang, A rapid detection of COVID-19 viral RNA in human saliva using electrical double layer-gated field-effect transistor-based biosensors, Adv. Mater. Technol. 7 (2022), 2100842.
[36] M.M. Bordbar, H. Samadinia, A. Sheini, J. Aboonajmi, H. Sharghi, P. Hashemi, H. Khoshsafar, M. Ghanei, H. Bagheri, A colorimetric electronic tongue for point-of-care detection of COVID-19 using salivary metabolites, Talanta 246 (2022), 123537.
[37] A.K. Sari, Y.W. Hartati, S. Gaffar, A review on the development of aptamer immobilization techniques in aptamer-based electrochemical biosensors for viruses detection, Anal. Bioanal. Electrochem. 14 (2022) 127–143.
[38] An RNA aptamer specific to Hsp70-ATP conformation inhibits its ATPase activity independent of Hsp40, Nucleic Acid Therapeut. 25 (2015) 103–112.
[39] H.D. Hill, C.A. Mirkin, The bio-barcode assay for the detection of protein and nucleic acid targets using DTT-induced ligand exchange, Nat. Protoc. 1 (2006) 324–336.
[40] K. Fu, S. Li, X. Jiang, Y. Wang, B.G. Willis, DNA gold nanoparticle nanocomposite films for chemiresistive vapor sensing, Langmuir 29 (2013) 14335–14343.
[41] Y. Wang, Z. Li, H. Yu, Aptamer-based Western blot for selective protein recognition, Front. Chem. 8 (2020), 570528.
[42] R.J. Trachman, A. Autour, S.C. Jeng, A. Abdolahzadeh, A. Andreoni, R. Cojocaru, R. Garipov, E.V. Dolgosheina, J.R. Knutson, M. Ryckelynck, Structure and functional reselection of the Mango-III fluorogenic RNA aptamer, Nat. Chem. Biol. 15 (2019) 472–479.
[43] A. Bard, Standard Potentials in Aqueous Solution, Routledge, 2017.
[44] M. Negahdary, L. Angnes, An aptasensing platform for detection of heat shock protein 70 kDa (HSP70) using a modified gold electrode with lady fern-like gold (LFG) nanostructure, Talanta 246 (2022), 123511.
[45] C. Cao, J. Liu, S. Tang, Z. Dai, F. Xiao, W. Rang, L. Liu, T. Chen, Y. Yuan, L. Li, Amplified electrochemical determination of UO22+ based on the cleavage of the DNAzyme and DNA-modified gold nanoparticle network structure, Microchim. Acta 187 (2020) 1–9.
[46] J.M. Carnerero, S. Masuoka, H. Baba, Y. Yoshikawa, R. Prado-Gotor, K. Yoshikawa, Decorating a single giant DNA with gold nanoparticles, RSC Adv. 8 (2018) 26571–26579.
[47] A.J. Bard, L.R. Faulkner, Fundamentals and applications, Electrochem. Methods 2 (2001) 580–632.
[48] J. Wang, Analytical Electrochemistry, Wiley, 2004.
[49] W. Junprung, P. Norouzitallab, S. De Vos, A. Tassanakajon, D. Nguyen Viet, G. Van Stappen, P. Bossier, Sequence and expression analysis of HSP70 family genes in Artemia franciscana, Sci. Rep. 9 (2019) 1–13.
[50] K.F. Amawi, I.S. Al-Mazari, A. Alsarhan, H.Q.M. Alhamad, A.J. Alkhatib, Diabetes upregulates the expression of HSP90 and downregulates HSP70 in the liver of diabetic rats, Comp. Clin. Pathol. 28 (2019) 473–478.
[51] S. Lim, H.Y. Cho, D.G. Kim, Y. Roh, S.-Y. Son, A.U. Mushtaq, M. Kim, D. Bhattarai, A. Sivaraman, Y. Lee, Targeting the interaction of AIMP2-DX2 with HSP70 suppresses cancer development, Nat. Chem. Biol. 16 (2020) 31–41.
[52] S. Zerikiotis, C. Angelidis, I. Dhima, K.K. Naka, P. Kasioumi, V. Kalfakakou, D. Peschos, P. Vezyraki, The increased expression of the inducible Hsp70 (HSP70A1A) in serum of patients with heart failure and its protective effect against the cardiotoxic agent doxorubicin, Mol. Cell. Biochem. 455 (2019) 41–59.
[53] M. Molanouri Shamsi, Z.M. Hassan, R. Gharakhanlou, Exercise-induced Chaperokine Activity of Hsp70: Possible Role in Chronic Diseases, Chaperokine Activity of Heat Shock Proteins, Springer, 2019, pp. 193–209.
[54] B.S. Rutledge, W.-Y. Choy, M.L. Duennwald, Folding or holding?—Hsp70 and Hsp90 chaperoning of misfolded proteins in neurodegenerative disease, J. Biol. Chem. 298 (2022).
[55] J.D. Vavilova, A.A. Boyko, N.I. Troyanova, N.V. Ponomareva, V.F. Fokin, E. Y. Fedotova, M.A. Streltsova, S.A. Kust, M.V. Grechikhina, O.A. Shustova, Alterations in proteostasis system components in peripheral blood mononuclear cells in Parkinson disease: focusing on the HSP70 and p62 levels, Biomolecules 12 (2022) 493.
[56] B. Sun, Y. Wang, D. Li, W. Li, X. Gou, Y. Gou, F. Hu, Development of a sensitive electrochemical immunosensor using polyaniline functionalized graphene quantum dots for detecting a depression marker, Mater. Sci. Eng. C 111 (2020), 110797.
[57] B. Sun, J. Cai, W. Li, X. Gou, Y. Gou, D. Li, F. Hu, A novel electrochemical immunosensor based on PG for early screening of depression markers-heat shock protein 70, Biosens. Bioelectron. 111 (2018) 34–40.
[58] B. Özcan, M.K. Sezgintürk, Graphene oxide based electrochemical label free immunosensor for rapid and highly sensitive determination of tumor marker HSP70, Talanta 160 (2016) 367–374.
[59] B. Demirbakan, M.K. Sezgintürk, A novel immunosensor based on fullerene C60 for electrochemical analysis of heat shock protein 70, J. Electroanal. Chem. 783 (2016) 201–207.
[60] N.H. Maniya, K. Parashar, L.N. Kadam, D.N. Srivastava, Electrochemical detection of heat shock protein 70 over cost-effective plastic chip electrode platform, J. Taiwan Inst. Chem. Eng. 128 (2021) 11–19.
[61] M.N. Sonuç Karaboğa, Ç.S. Şimşek, M.K. Sezgintürk, AuNPs modified, disposable, ITO based biosensor: early diagnosis of heat shock protein 70, Biosens. Bioelectron. 84 (2016) 22–29.
[62] M. Nycz, K. Arkusz, D.G. Pijanowska, Fabrication of electrochemical biosensor based on titanium dioxide nanotubes and silver nanoparticles for heat shock protein 70 detection, Materials 14 (2021) 3767.
[63] N.H. Maniya, D.N. Srivastava, Fabrication of porous silicon based label-free optical biosensor for heat shock protein 70 detection, Mater. Sci. Semicond. Process. 115 (2020), 105126.
[64] R. Denomme, A Label-free Biosensor for Heat Shock Protein 70 Using Localized Surface Plasmon Resonance, University of Waterloo, 2012.
[65] X. Ding, H. Li, H. Xie, Y. Huang, Y. Hou, Y. Yin, G. Li, A novel method to assay molecular chaperone activity of HSP70: evaluation of drug resistance in cancer treatment, Biosens. Bioelectron. 47 (2013) 75–79.